Journal of Physics: Conference Series **305** (2011) 012092 doi:10.1088/1742-6596/305/1/012092

Parameter subset selection based damage detection of aluminium frame structure

B Titurus[1] **and MI Friswell**[2]
[1] Department of Aerospace Engineering, University of Bristol, Queens Building, University Walk, Bristol, BS8 1TR, U.K.
[2] College of Engineering, Swansea University, Singleton Park, Swansea SA2 8PP, U.K.

E-mail: brano.titurus@bristol.ac.uk, m.i.friswell@swansea.ac.uk

Abstract: A three storey aluminium frame structure was tested in multiple damage cases. All damage scenarios, simulated by the localized stiffness changes, were associated with joint areas of the structure. Further, between damage tests the structure was returned to its healthy reference conditions and was again measured. In this paper, a parameter subset selection methodology is applied to an updated finite element model of the structure, together with a previously demonstrated approach employing concepts of model sensitivity subspace angles, first order model representation and mixed response residuals for damage detection. The objective of this paper is the evaluation of these methods on a real experimental structure with significant complexity, represented by an imprecise reference mathematical model and in the environment with uncertain reference structural state. The questions of symmetry, mixed response residuals and semi-localized parameterization are also addressed in this work.

1. Introduction

Vibration-based damage detection has potential to form a part of integrated health monitoring sub-systems in spatially extended mechanical systems. A useful feature of this approach is its global nature to detect changes in the composition and distribution of three basic structural properties; mass, damping and stiffness; and the effect of their changes on measurable and identifiable dynamic properties such as modal properties. Changes in the modal properties are attributable to the changes in basic structural properties, such as stiffness, or specific damage event in the mechanical system.

The two major problems associated with this approach are: (i) limited quality, quantity, autonomy (e.g. unknown system inputs) and relevancy (e.g. sensitivity of the observed modal information) of the measured data, and (ii) linearity assumptions inherent in this method. Recent developments in measurement and identification techniques address many experimental aspects of these problems. Questions of relevancy are still being studied and are partially addressed in this paper. Ultimately, structural damage is mostly associated with nonlinear modes of operation, such as cracks, friction, etc. However, the use of "small vibrations" allows the use of the above-mentioned methodology even in these situations. In the current study the choices are made such that potential nonlinearities may affect detection and intermediate results.

The concept of parameter subset selection was originally applied in the context of model updating in [1]. Friswell et al. [2] used subset selection for damage detection and location. Titurus et al. [3] gave a practical demonstration of this damage location methodology. Titurus and Friswell [4] further theoretically expanded the method and Yun et al. [5] gave a more recent application of subset selection. It is important to note that the original use of subset selection strategies was in statistics for regression [6].

The objective of this paper is to evaluate parameter subset selection ideas in vibration-based damage detection in the realistic context of medium complexity. The structure of choice is an

aluminium three-story Meroform structure as previously studied by the authors for model updating [7]. In the current paper the three damage levels are considered. Damage was simulated by loosening one end of a strut linked to a specific aluminium node. Multiple damage levels were obtained by increasing the extent of looseness in the joint. The model based damage detection approach applied in this paper utilises two fundamental concepts: model parameterisation and model updating [8]. These two concepts are further augmented with the damage detection approach utilising a linearized response model and parameter subset selection [2], [3], [4]. The key element linking the model updating and damage detection parts of the algorithm is the reparameterisation. This represents the transition from the updated to the validated model, with its updating-oriented parameterisation, to a new, damage detection-oriented parametric description. Parameter values in the reparameterised part of the algorithm are based on the reference and, whenever applicable, updated model representations.

2. Parameterised response models

In both updating and damage detection, the behaviour of the model is described by the response vector $\mathbf{z} \in \mathbb{R}^{N_Z}$ with N_Z elements chosen from the available measurable set of model responses. This arrangement represents a response model of the system or structure and is parameterised with a suitable set of parameters. In the current research two parameterisations are applied, an updating parameterisation $\mathbf{p} \in \mathcal{D}_1 \subseteq \mathbb{R}^{N_P}$ and a damage detection parameterisation $\mathbf{d} \in \mathcal{D}_2 \subseteq \mathbb{R}^{N_D}$.

Many analytical techniques rely on the Taylor series expansion of the nonlinear response model around its reference state, i.e. parameter $\mathbf{p}_k$

$$\mathbf{z}_m = \mathbf{z}(\mathbf{p}_k) + \mathbf{S}_k(\mathbf{p} - \mathbf{p}_k) + O(|\mathbf{p} - \mathbf{p}_k|^2),\ \mathbf{S}(\mathbf{p}) = \left[\partial z_i(\mathbf{p}) / \partial p_j\right] \in \mathbb{R}^{N_Z \times N_P}. \tag{1}$$

An equation identical to (1) can be written for the alternative parameterisation $\mathbf{d} \in \mathcal{D}_2 \subseteq \mathbb{R}^{N_D}$.

3. Model updating and damage detection

In model updating, the objective is to modify the model $\mathbf{z} = \mathcal{Z}(\mathbf{p})$ with respect to the measured responses $\mathbf{z}_m$ such that $L(\mathcal{Z}(\mathbf{p}), \mathbf{z}_m) \to \min$, where $L(\mathbf{a}, \mathbf{b})$ is the distance measure between the vectors $\mathbf{a}$ and $\mathbf{b}$, e.g. $(\mathbf{a}-\mathbf{b})^T \mathbf{W} (\mathbf{a}-\mathbf{b})$. Model updating is the inverse problem of finding a suitable parameter instance such that $\mathbf{p}_m \approx \mathcal{Z}^{-1}(\mathbf{z}_m)$, where $\mathcal{Z}^{-1}$ is the inverse map, which is usually a non-unique and ill-posed operator or response-parameter map.

Neglecting higher order quantities, representation (1) enables the baseline iterative model inversion

$$\mathbf{p}_{k+1} = \mathbf{p}_k + \mathbf{S}_k^+ (\mathbf{z}_m - \mathbf{z}_k) \tag{2}$$

where $\mathbf{S}_k^+$ is the pseudo-inverse of the matrix $\mathbf{S}_k$.

The source of activity in the formulations based on equation (2) is the initial residual response residual vector $\Delta \mathbf{z}_U = \mathbf{z}_m - \mathbf{z}_0$. Similarly, the source of activity in the case of damage detection is the response residual defined as $\Delta \mathbf{z}_D = \mathbf{z}_m - \mathbf{z}_{ref}$, where $\mathbf{z}_{ref}$ is the model reference response. The current work assumes that $\mathbf{z}_{ref} = \tilde{\mathbf{z}}$, where $\tilde{\mathbf{z}}$ is the undamaged response vector.

The following relationship can be defined for the measured/observed response vector with the damage detection oriented parameterisation $\mathbf{d} \in \mathcal{D}_2 \subseteq \mathbb{R}^{N_D}$

$$\mathbf{z}_m \approx \mathbf{z}_{ref} + \mathbf{L}_U \Delta \mathbf{d}_D. \tag{3}$$

The approximate linearised model, with the new sensitivity matrix $\mathbf{L}$, for damage induced response residual suitable for the application with parameter subset selection theory is

$$\mathbf{L}_U \Delta \mathbf{d}_D \approx \mathbf{z}_m - \mathbf{z}_{ref} \equiv \Delta \mathbf{z}_D,\ \mathbf{L}_U = \left[\partial z_i(\mathbf{d}_U) / \partial d_j\right] \in \mathbb{R}^{N_Z \times N_D}. \tag{4}$$

4. Partitioning the damage detection equation

Equation (4) is the basis for the damage location algorithm [2] utilising the theory of parameter subset selection [6]. A small set of parameters $d_{D,i}$ is searched that produces a linear combination of the column sensitivity vectors $\mathbf{l}_{U,i}$, $\mathbf{L}_U=[\mathbf{l}_{U,i}]$, such that the following cost function is minimised $J_{SS}=\|\sum_{i=1}^{N_{SS}}\Delta d_{D,i}\mathbf{l}_{U,i}-\Delta\mathbf{z}_D\|$, assuming that $N_{SS}\ll N_D$. A limited spatial extent of the damage translates into changes in a small set of parameters associated with the damage region. The computations associated with J_{SS} can be based on iterative procedures combining forward selection with Efroymson's algorithm [2], [6]. This paper considers a simplified form of this methodology and looks only at the first iteration with *subspace angles* based on the cost function J_{SS}. Subspace angles will be evaluated between the response residuals and suitable sensitivity matrix subspaces.

The column-wise partitioned form of the sensitivity matrix $\mathbf{L}_U$ will be adopted based on the established joint-parameter associations

$$\begin{gathered}\mathbf{L}_U=\left[\mathbf{L}_1^J,\mathbf{L}_2^J,\ldots,\mathbf{L}_{n_J}^J\right],\quad \mathbf{L}_k^J=\left[\frac{\partial\mathbf{z}}{\partial d_1^{J_k}},\frac{\partial\mathbf{z}}{\partial d_2^{J_k}},\ldots,\frac{\partial\mathbf{z}}{\partial d_{m_k}^{J_k}}\right]\\ \Delta\mathbf{d}=\left[\Delta\mathbf{d}_1^T,\Delta\mathbf{d}_2^T,\ldots,\Delta\mathbf{d}_{n_J}^T\right]^T,\ \Delta\mathbf{d}_k=\left[\Delta d_1^{J_k},\Delta d_2^{J_k},\ldots,\Delta d_{m_k}^{J_k}\right]^T,\ N_D=\sum_{k=1}^{n_J}m_k\end{gathered}\tag{5}$$

where n_J represents the number of joints in the model, J_k identifies *k*-th joint and m_k represents the number of parameters associated with *k*-th joint with the total number of the parameters equal to N_D.

Parameters in the set describing the joint J_k will be called the *k*-th *joint parameters* and the corresponding column vectors of the sensitivity matrix assembled in the matrix $\mathbf{L}_k^J\in\mathbb{R}^{N_Z\times m_k}$ will form the *k*-th *joint (sensitivity) subspace* $\mathcal{J}_k=\{\mathbf{L}_k^J\mathbf{d}_k:\mathbf{d}_k\in\mathbb{R}^{m_k}\}$. The ability of the *k*-th joint subspace to "explain" the response residuals $\Delta\mathbf{z}_D$ will be determined by the (principal) subspace angles

$$\beta_k=\angle\left(\mathcal{J}_k,\Delta\mathbf{z}_D\right),\quad \beta_k\in\langle 0°,90°\rangle.\tag{6}$$

Finally, because of the use of multiple response types, a relative weighting is applied such that original problem (4) can be described by the following block matrix equation

$$\begin{bmatrix}(1-\alpha)\mathbf{I}_{N_\lambda} & \mathbf{0}\\ \mathbf{0} & \alpha\mathbf{I}_{N_\phi}\end{bmatrix}\begin{bmatrix}\mathbf{L}_{1,\lambda}^J & \mathbf{L}_{2,\lambda}^J & \cdots & \mathbf{L}_{N_J,\lambda}^J\\ \mathbf{L}_{1,\phi}^J & \mathbf{L}_{2,\phi}^J & \cdots & \mathbf{L}_{N_J,\phi}^J\end{bmatrix}\Delta\mathbf{d}_D=\begin{bmatrix}(1-\alpha)\Delta\mathbf{z}_\lambda\\ \alpha\Delta\mathbf{z}_\phi\end{bmatrix}\tag{7}$$

where $\alpha\in\langle 0,1\rangle$ represents the relative weight between the two response types, matrices $\mathbf{L}_{k,\lambda}^J\in\mathbb{R}^{N_\lambda\times m_k}$ and $\mathbf{L}_{k,\phi}^J\in\mathbb{R}^{N_\phi\times m_k}$, N_λ is the number of frequency responses, N_λ is the number of mode shape responses, $N_\phi+N_\lambda=N_Z$. The use of a weighting factor means that $\mathcal{J}_k=\mathcal{J}_k(\alpha)$ and $\beta_k=\beta_k(\alpha)$. While determination of the weighting factor α is not straightforward, it does not constitute the main interest of this paper and uncertainty associated with this parameter will be addressed only by using multiple values of this parameter when evaluating subspace angles.

5. Case study

5.1. Experimental conditions and finite element model

A number of EMA experiments were performed to acquire and identify healthy and damage affected modal responses. The experiments were performed on the three-bay aluminium Meroform M12

structure shown in figure 1(a). Details of a joint are shown in figure 1(b). The corresponding analytical responses and other calculations were performed in Matlab with the help of an in-house Finite Element (FE) code. The model of the structure is shown in figure 1(c). The numbers in this figure identify joint numbers and damage location is identified by an arrow in the same figure.

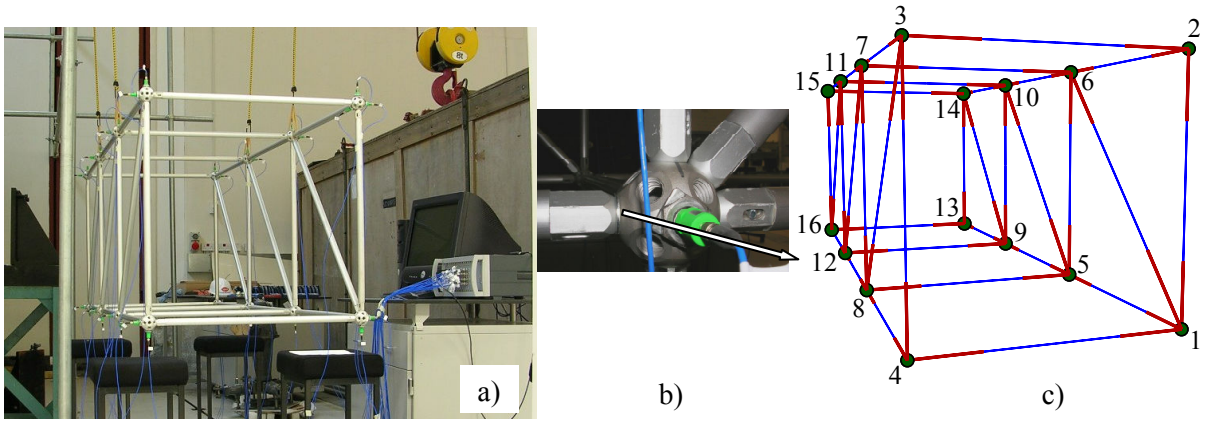

Figure 1. Three-bay aluminium frame structure: a) experimental setup for EMA, b) detail of a joint, c) FE model with joint numbers (the affected connection identified with the arrow).

The model of the structure consists of 168 elements (3D Euler-Bernoulli beams, point masses and rigid links) with total of 708 DOFs. The material properties chosen are those of standard aluminium, and the model is unconstrained. During the experiment, the structure was supported in free-free conditions and was instrumented with 33 single-axis B&K accelerometers. The data acquisition and EMA data processing were performed with an LMS measurement system. During the test, the structure was repetitively excited with an impact hammer to allow identification of all 33 FRFs and the mode shapes and natural frequencies were extracted.

5.2. Model parameterisation and reparameterisation

The model presented in figure 1(c) was initially parameterised for model updating purposes. Three global stiffness-related parameters were chosen to accommodate differences resulting from model uncertainties, Table 3.

Damage-oriented reparameterisation links a number of parameters with all joint regions in the frame structure. All beam elements linked with aluminium nodes (modelled as discrete masses) have parameterised Young's modulus, with its value determined in the previous model updating. Overall 68 elements (partially rigid 3D beam elements) were parameterised and attributed to 16 joint groups dependent of the model topology shown in figure 1(c). The sensitivity analyses produced sensitivity matrices $\mathbf{S}_k = \mathbf{S}(\mathbf{p}_k) \in \mathbb{R}^{8\times 3}$ and $\mathbf{L}_U = \mathbf{L}(\mathbf{p}_U \to \mathbf{d}_U) \in \mathbb{R}^{N_Z \times 68}$, where $N_Z \in \langle 8, 264 \rangle$.

5.3. Modal analysis and damage cases

The damage mode considered in this paper is a single *loosened bolted connection*. Three levels of damage were obtained by mechanical loosening the bolted connection associated with node 12 (figures 1(b) and 1(c)). This connection was originally tightened to nominally the same extent as all of the other connections. In total, 11 healthy measurements were completed at the beginning and in between the damage tests. Figure 2 shows point Frequency Response Functions (FRFs) collected during the multiple healthy and damage tests. Three damage levels were introduced by loosening of the connection indicated in figure 1(b) as follows: (i) Damage case 1 by unscrewing the hexagonal nut by 20º, (ii) Damage case 2 by an incremental increase of the unscrewing angle by 15º, and (iii) Damage case 3 by an incremental increase of the unscrewing angle by an additional 40º. Previously to this, the four complete nominal or healthy EMA experiments were completed.

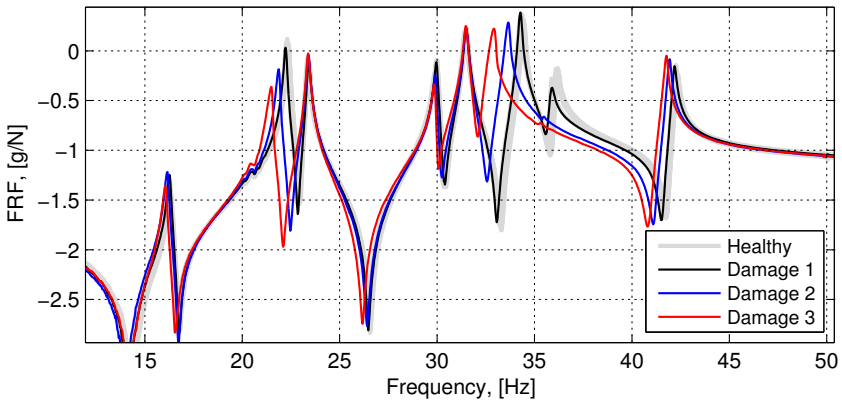

Figure 2. Comparison between identified point FRFs.

Table 1 summarises the results of these tests. The column identified as *healthy* represents the arithmetic mean of the ten nominal EMA experiments, while the columns identified as Damage 1, Damage 2 and Damage 3 present the actual damage tests.

Table 1. Natural frequency comparison between measured healthy and damage cases.

	Identified natural frequencies, [Hz]				Differences, 100×(D-H)/H, [%]		
NF number	Healthy (H)	Damage 1 (D1)	Damage 2 (D2)	Damage 3 (D3)	Difference D1-H	Difference D2-H	Difference D3-H
1	16.27	16.26	16.13	16.02	-0.06	-0.86	-1.54
2	22.28	22.21	21.83	21.41	-0.31	-2.02	-3.90
3	23.35	23.40	23.39	23.37	0.21	0.17	0.09
4	29.92	29.96	29.91	29.85	0.13	-0.03	-0.23
5	31.44	31.49	31.48	31.48	0.16	0.12	0.13
6	34.32	34.25	33.59	32.78	-0.20	-2.13	-4.49
7	36.02	35.81	35.40	35.24	-0.58	-1.72	-2.17
8	42.25	42.17	41.90	41.72	-0.19	-0.83	-1.25

The second part of Table 1 compares all three damage cases with respect to the healthy averaged case. The two modes particularly sensitive to the introduced damage are modes 2 and 6. A better understanding of the sensitivity of these modes, as opposed to the relative insensitivity of modes 3, 4 and 5, can be inferred from the associated mode shapes, shown in figure 3.

Figure 3 provides a complete summary of the differences in identified natural frequencies with respect to the averaged healthy frequencies. This information is provided on the horizontal axes of each individual subplot, where each subplot summarises information for single identified mode. Moreover, all eleven individual identified healthy test cases and their respective natural frequencies are included and compared to their mean. The vertical axis of each subplot shows the identified modal damping ratio. All subplots, with exception of the mode 1, share common scaling and limits. An effective lack of stationarity due to bolted connections is reflected in the damping variability observed particularly in mode 1. Despite a reasonable extent of the modifications and repeated loosening and tightening in any location of the structure, as conducted between healthy cases, relatively low variability is observed between healthy cases, documented by the standard deviations σ provided in Figure 3, with clear distinction between healthy and damage cases D2 and D3. The case D1, according to this figure may not produce changes sufficiently large to enable successful damage detection.

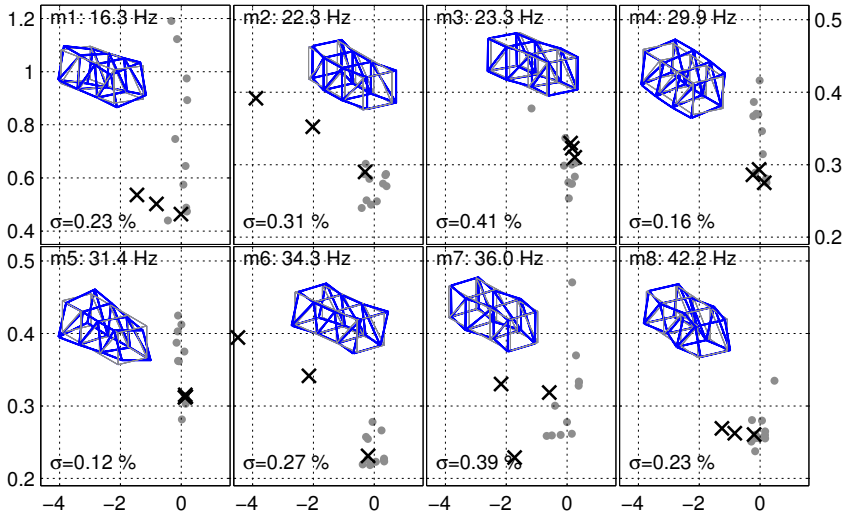

Figure 3. Identified natural frequencies and modal damping, horizontal axes represent relative NF differences [%], vertical axes represent modal damping [%] (H: dot markers, D: cross markers).

Figure 3 clearly shows that the increased sensitivity in modes 2 and 6, as observed in Table 1, and the relative insensitivity of modes 3, 4 and 5, is inherently linked to their corresponding mode shapes. Increased local curvature of the mode shape in the vicinity of the damage location translates into increased sensitivity of the corresponding natural frequency. In contrast is mode 5, as shown in figure 3, with little curvature near the damage location.

5.4. Model updating

The FE model is described in Section 5.1. The updating algorithm used the first 8 natural frequency residuals with the cost function $J_{UP}=\sum_{i=1}^{8}(z_{m,i}-z_i(\mathbf{p}))/z_{m,i}$, where $\mathbf{p}\in\mathbb{R}^3$ and $\mathbf{S}(\mathbf{p})\in\mathbb{R}^{8\times3}$. The parameters selected for this updating exercise reflected the positive biased character of the initial response residuals $\mathbf{z}_m-\mathbf{z}(\mathbf{p}_0)$, Table 2, indicating the FE model was too stiff. Three global stiffness parameters were selected: Young's modulus E for all semi-rigid Euler-Bernoulli beam elements (thick red lines in figure 1c)) and two sectional moments of inertia, I_Y and I_Z, for all remaining standard Euler-Bernoulli elements (thin blue lines in figure 1c)). Results of the updating study are summarised in Table 2 for the natural frequency values and in Table 3 for the parameter values.

Table 2. Comparison between measured, reference (FEM1) and updated natural frequencies (FEM2).

	Identified natural frequencies, [Hz]			Differences, [%] 100×(FEM-EXP)/EXP	
NF number	Mean EMA EXP	FE model 1 FEM1	FE model 2 FEM2	Difference FEM1-EXP	Difference FEM2-EXP
1	16.27	18.21	16.32	11.92	0.31
2	22.28	25.40	22.25	14.00	-0.13
3	23.35	26.83	23.44	14.90	0.39
4	29.92	34.45	30.04	15.14	0.40
5	31.44	36.09	31.59	14.79	0.48
6	34.32	38.63	34.01	12.56	-0.90
7	36.02	41.14	36.00	14.21	-0.06
8	42.25	47.59	41.80	12.64	-1.07

Model updating was performed with respect to the averaged healthy responses and the initial response residuals were reduced from the interval (12,15) % to approximately (-1,0.5) %. Despite not using any additional regularisation or constraint conditions, the changes in the two sectional moments of inertia were very small and similar to each other, confirming the initial confidence and nominal sectional symmetry associated with these parts of the structure. The major change was associated with joint regions and represented effective stiffness reduction due to the presence of the mechanical joint. More details of this study are provided in [7].

Table 3. Summary of the parameter changes after model updating.

		Parameter values		Differences, [%] 100×(U-R)/R
ID	Name, [units]	Reference	Updated	Difference
1	I_Y, [m^4]	3.63679E-9	3.80706E-9	4.68
2	I_Z, [m^4]	3.63679E-9	3.74096E-9	2.86
3	E, [Pa]	7.0E+10	4.97125E+10	-28.98

5.5. Damage detection results

Figure 1(c) shows the joint numbering used in the following bar graphs. Element 136 is the location of the damage, and is adjacent to joint 12 on the member connected to joint 16. Figure 4 shows the subspace angles β_k, $k=1,\ldots,16$, introduced in Section 4. These are the angles between three response residuals $\Delta\mathbf{z}_{D,1}$, $\Delta\mathbf{z}_{D,2}$, $\Delta\mathbf{z}_{D,3}$, associated with D1, D2, D3 cases, respectively, and all joint subspaces $\mathcal{J}_k$, $k=1,\ldots,16$. Response residuals $\Delta\mathbf{z}_{D,i}\in\mathbb{R}^8$ are based on measured natural frequencies.

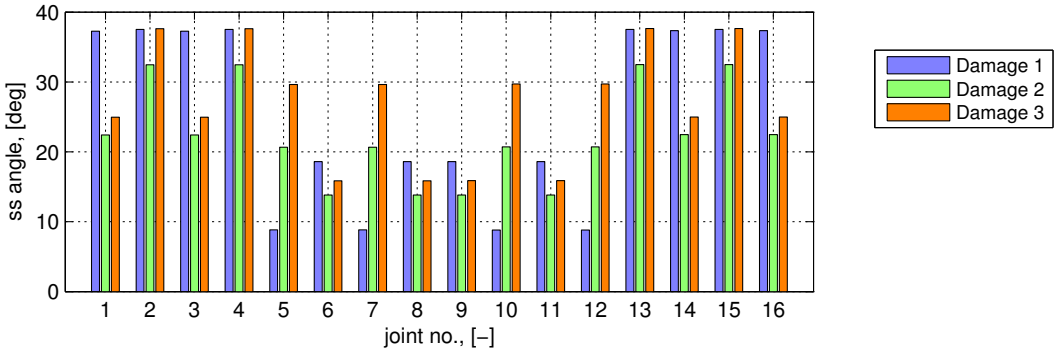

Figure 4. Subspace angles between joint subspaces and natural frequency response residuals.

Structural symmetry, both on the geometric and parametric level, combined with the global nature of the response residuals used in this case is reflected in the obtained results. For the case D1 the joints with smallest subspace angles are joint 5, 7, 10 and 12. The symmetry problem is addressed later in the paper by using mode shapes. Further, more detailed analysis regarding the success of case D1 as opposed to the problems associated with cases D2 and D3, when using only natural frequencies, is discussed in association with figures 6 and 7.

Figure 5 complements the results provided in figure 4 by showing the breakdown of the subspace angles between all parameterised element sensitivity subspaces and the three available natural frequency residual vectors. The five elements directly associated with joint 12 are identified by black arrows. First 32 bar graph triples are associated with transverse joint elements, following three groups of elements between 100 and 145, each constituted by 8 bar graph triples, are associated with longitudinal joint elements with each group representing one bay of the structure. The final block of elements between 148 and 171 corresponds to the diagonal joint elements.

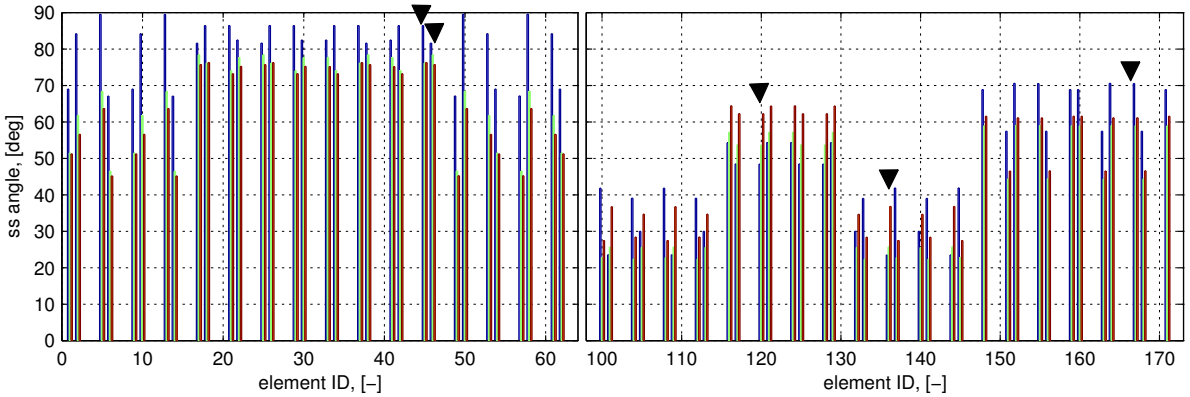

Figure 5. Subspace angles for individual element subspaces (D1: blue bars, D2: green bars, D3: orange bars; black triangles indicate individual elements associated with joint 12).

Figure 5 also suggests problems with symmetry, however, when considering only elements corresponding to joint 12 (black triangles), element 136 is clearly the one with the lowest subspace angles within its own joint group.

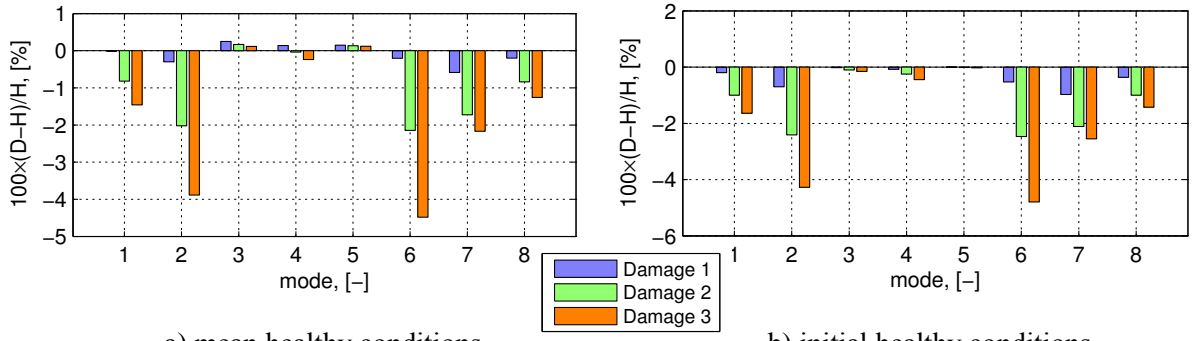

a) mean healthy conditions b) initial healthy conditions

Figure 6. Identified NF residuals defined with respect to the healthy conditions.

The results for case D1 seem to indicate the correct *joint subset* (owing to the global nature of the residuals used). However, the natural frequency changes in D1 case seem to be low, –0.58 % at most, and in some cases even positive, see figure 6(a) Two important facts associated with this figure are that: (i) real values of the residuals retain a decreasing trend with increasing damage, (ii) the *averaged* natural frequencies are used in response calculations. Figure 6(b) shows the natural frequency residuals calculated with respect to the healthy state measured immediately before the start of the damage studies. This figure shows two important facts: (i) in this case all residuals are negative (even though some of them are very low due to relative mode insensitivity) with the frequencies having a decreasing trend due to stiffness reduction when increasing damage level, (ii) the pattern of the residuals for D1 case is similar between figures 6(a) and 6(b).

The apparent lack of success in cases D2 and D3 is analysed with the support of figure 7. This figure presents simulation of the considered damage case for element 136 with the same parameter type as used in figures 4 and 5, i.e. a Young's modulus reduction. The figure shows the relative reduction in natural frequencies when *increasing* the damage level by *reducing* the Young's modulus of element 136. Two important observations can be made in relation to above analysis: (i) the pattern of the changes of the response residuals in this analytical case is comparable with changes observed in figure 6, and (ii) even extreme damage levels represented by a 80% Young's modulus reduction produces a reduction in the second natural frequency of approximately 2%, as opposed to a 4% reduction in the experiment. This implies that Young's modulus reduction provides a suitable

representation of the damage for range of frequencies considered, however, the parametric variations needed to capture the real changes do not correspond to the linear assumption associated with the theory given in Sections 3 and 4. This is, possibly, a reason behind the lack of success of this methodology for cases D2 and D3, in contrast to the success in case D1, i.e. a small damage.

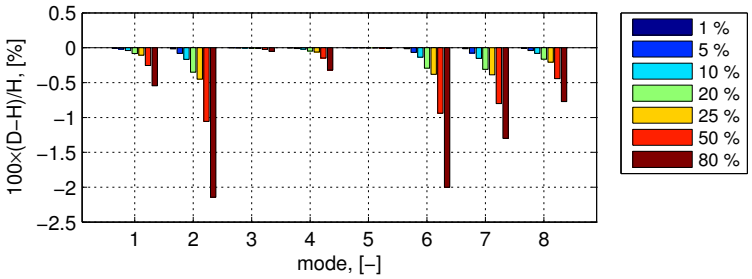

Figure 7. Computed NF residuals. Element 136 "damaged" by reducing its Young's modulus.

Symmetry related detection problems demonstrated in figure 4 can be overcome with the use of more localised responses such as mode shapes. Figure 8 shows the subspace angles corresponding to a response residuals based on the first 8 natural frequencies and all 32 components of mode 6, leading to the residual vectors $\Delta\mathbf{z}_{D,i}\in\mathbb{R}^{40}$. This case uses $\alpha=0.7$, selected such that the initial effect of the natural frequencies, $\alpha=0$, is balanced with the effect of the mode shape component residuals, $\alpha=1$. This figure suggests that the use of the mode shape improves the localisation properties of the resulting subspace angles and indicates potential damage locations as joints 7 and 12 for case D1. However, problems with the excessive damage levels in cases D2 and D3 remain.

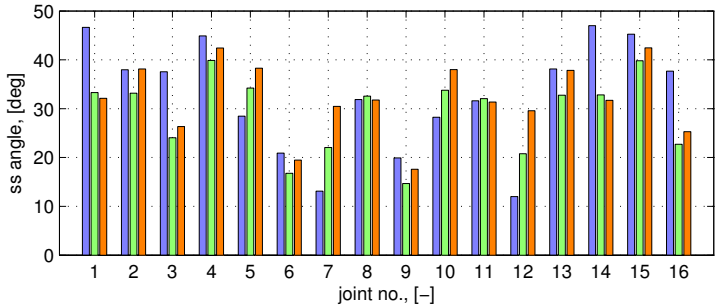

Figure 8. Computed subspace angles between joint subspaces and mixed response residuals (8 natural frequencies and 32 components of mode 6), α=0.7.

Figure 9 shows the case where all eight modes are included, i.e. $\Delta\mathbf{z}_{D,i}\in\mathbb{R}^{264}$. When using $\alpha=0.7$, as for figure 8, the indication for damage is associated with joint 12, instead of joint 7, as joint 12 has a slightly lower subspace angle between its joint subspace and $\Delta\mathbf{z}_{D,1}$. Figure 10 also shows results of the study with $\Delta\mathbf{z}_{D,i}\in\mathbb{R}^{264}$ and $\alpha=0.99$, i.e. the information provided by the mode shape residual dominates in the subspace angle calculations. The use of mode shape residuals in case D1 still produces correct damage location estimation, however, with decreased resolution capacity, possibly, due to the use of a less accurate response type. Moreover, it is interesting to evaluate cases D2 and D3, both with respect to this study, and also in contrast to the study presented with figure 6 and 7. Firstly, increased damage levels seem to produce more distinctive mode shape response residuals overcoming initially dominating mode shape identification uncertainties. Secondly, the generally acknowledged lower response sensitivities of the mode shapes seem to work better for the given parameterisation type and the large damage levels, where the correct damage location, joint 12, is identified for both cases D2 and D3.

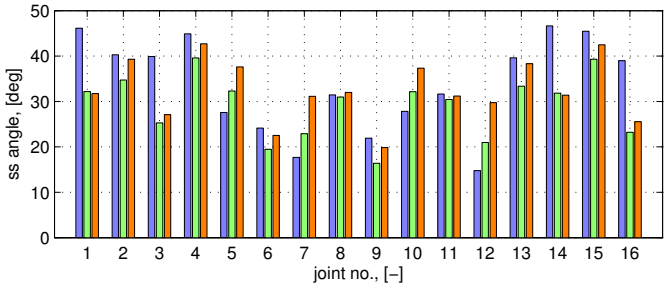

Figure 9. Computed subspace angles between joint subspaces and mixed response residuals (8 natural frequencies and 32 components of modes 1 to 8), α=0.7

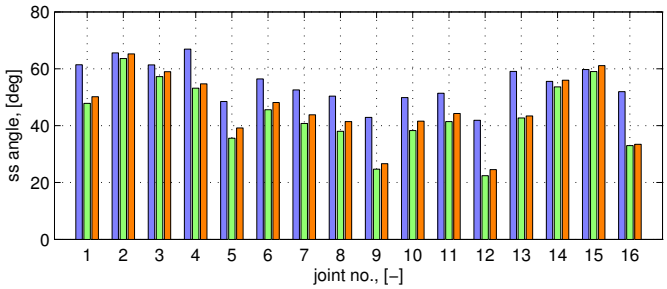

Figure 10. Computed subspace angles between joint subspaces and mixed response residuals (8 natural frequencies and 32 components of modes 1 to 8), α=0.99.

6. Conclusion

The paper demonstrates the use of parameter subset selection in damage detection on a medium complexity, real case study. Moreover, the paper also applies a novel theoretic and algorithmic approach to the use of subset selection, namely, the use of joint sensitivity subspaces and the concept of reparameterisation as integral step during transition from model validation and updating towards parameter-based damage detection. Significant bias in considered responses, whether due to identification errors or large uncertainty in the healthy state of the structure, can negatively affect localisation capability of this algorithm.

The experimental case study provided a detailed analysis of the use, limitations and possible ways forward associated with the application of different residual types and geometric and parametric symmetries. The use of reparameterisation is successfully demonstrated in establishing a high-quality reference for further damage detection studies using *experimental residuals*. The damage is shown to induce large parametric variations in some cases, rendering the applied methodology not fully suitable. The mixing of mode shape response residuals with natural frequency residuals enables the symmetry and large parameter variation problems to be overcome. It was also shown that good knowledge of the healthy case enabled correct damage detection through the use of the representative modal residuals.

References

[1] Lallement G and Piranda J 1990 *Proc 8th IMAC* 579.
[2] Friswell MI, Penny JET and Garvey SD 1997 *Inverse Probl Eng* **5** 189.
[3] Titurus B, Friswell MI and Starek L 2003 *Comput Struct* **81** 2287.
[4] Titurus B and Friswell MI 2004 *Proc ISMA 2004* 545.
[5] Yun GJ, Ogorzalek KA, Dyke SJ and Song W 2010 *Struct Control Hlth* **17** 48.
[6] Miller AJ 2002 *Subset Selection in Regression*, 2nd edition (Chapman & Hall/CRC).
[7] Titurus B and Friswell MI 2010 *Proc ISMA 2010* 2701.
[8] Mottershead JE, Link M and Friswell MI 2011 *Mech Syst Signal Pr*, in press, doi:10.1016/j.ymssp.2010.10.012